

Sensing-Enhanced Handover Criterion for Low-Altitude Wireless Networks (LAWNs)

Jingli Li, *Student Member, IEEE*, Yiyan Ma, *Member, IEEE*, Bo Ai, *Fellow, IEEE*,
 Qingqing Cheng, *Member, IEEE*, Guoyu Ma, *Member, IEEE*, Mi Yang, *Member, IEEE*,
 Yunlong Lu, *Member, IEEE*, Wenwei Yue, *Member, IEEE*, and Zhangdui Zhong, *Fellow, IEEE*.

Abstract—With the rapid growth of the low-altitude economy, the demand for cellular-enabled low-altitude wireless networks (LAWNs) is rising significantly. The three-dimensional mobility of unmanned aerial vehicles (UAVs) will lead to frequent handovers (HOs) in cellular networks, while traditional reference signal received power (RSRP)-based criteria may fail to capture the dynamic environment, causing redundant HOs or HO failures. To address this issue and motivated by the underutilization of sensing information in conventional HO mechanisms, we propose a novel HO activation criterion for UAV systems that integrates both sensing parameters provided by integrated sensing and communication (ISAC) signals and RSRP. First, we construct an ISAC signal model tailored for low-altitude scenarios and derive the Cramér–Rao lower bound for sensing distance estimation. Subsequently, we propose a novel joint HO criterion that extends the conventional RSRP-based method by integrating sensing information from ISAC signals, enabling more reliable HOs in dynamic UAV environments. Simulation results show that the joint HO criterion outperforms the baseline RSRP-based criterion under different signal-to-noise ratio (SNR) and sensing pilot ratio conditions. Particularly, when $\text{SNR} \geq 0$ dB and the sensing pilot ratio is 20%, the proposed joint HO criterion reduces the average HO region length by 49.97% and improves the activation probability by 76.31%.

Index Terms—LAWNs, ISAC, Handover, CRLB.

I. INTRODUCTION

The rapid growth of low-altitude economy has steadily increased the demand for reliable low-altitude wireless networks (LAWNs) to support unmanned aerial vehicle (UAV). Advanced cellular technologies, such as 5G-A and 6G, are expected to play a pivotal role in supporting these requirements [1]. Due to the relatively simplified radio propagation environment at low altitudes, the UAV wireless channel is predominantly characterized by line-of-sight (LoS) propagation, creating favorable conditions for integrated sensing and communication (ISAC) applications [2]. ISAC enables UAV systems to simultaneously sense environmental parameters, such as delay and Doppler shifts from surrounding objects, while transmitting data [3]. Consequently, UAV systems supported by ISAC can achieve enhanced environmental awareness while effectively utilizing sensing information to further improve communication reliability.

Jingli Li, Yiyan Ma, Bo Ai, Guoyu Ma, Mi Yang, Yunlong Lu, and Zhangdui Zhong are with the School of Electronic and Information Engineering, Beijing Jiaotong University, Beijing 100044, China. Qingqing Cheng is with Queensland University of Technology, Brisbane, QLD 4000, Australia. Wenwei Yue is with the State Key Laboratory of Integrated Services Networks, Xidian University, Xi’an, Shaanxi 710071, China.

In LAWNs, handover (HO) is a critical component in maintaining communication performance. The current 3GPP standard for 5G NR typically employs various events based on reference signal received power (RSRP) to trigger HO in traditional UAV systems [4]. However, in low-altitude scenarios involving high mobility and altitude variation, it struggles to cope with rapid channel fluctuations, resulting in redundant or failed HOs [5]. Compared to the traditional RSRP-based HO decision mechanism, ISAC introduces a spatial sensing dimension, providing a richer information basis for HO decisions. However, existing HO procedures remain largely tailored to traditional communication systems and have yet to fully utilize sensing capabilities offered by ISAC [4]. Therefore, integrating ISAC sensing into the HO mechanism to enhance HO performance is a promising topic for LAWNs.

To improve HO performance in cellular-connected UAV scenarios, current studies have incorporated geometric or mobility information into RSRP-based HO mechanisms [5], [6]. However, such methods rely on external positioning systems, leading to extra hardware requirements and increased signaling overhead. Given the limitation, ISAC has gained attention for its ability to support concurrent sensing and communication within a unified framework. Towards that end, Meng *et al.* [2] developed a multi-BS cooperative localization mechanism to improve HO success rates by exploiting sensing information provided by ISAC, while Ge *et al.* [7] designed a distributed HO based on trajectory sharing that enhances connection continuity, demonstrating the feasibility of applying ISAC to HO decision-making. However, existing studies have not thoroughly explored sensing-driven HO criteria or modeling the impact of sensing errors on HO behavior.

To bridge this gap, we propose a novel HO criterion that integrates sensing distance provided by ISAC signals and RSRP, with the main contributions summarized as follows:

- We establish an ISAC signal model tailored to low-altitude scenarios and derive the Cramér–Rao lower bound (CRLB) for distance estimation. Based on the CRLB, we quantify the distance estimation error, serving as a foundation for designing a sensing-based HO criterion.
- A joint HO criterion is proposed by integrating the sensing distance parameter and RSRP, which triggers an HO whenever either criterion is met. By incorporating distance information, the proposed approach improves the HO success rate compared to RSRP-based methods.
- Simulation results show that, compared to the baseline

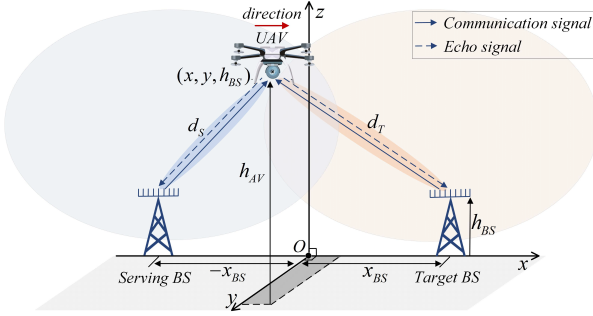


Fig. 1. G2A geometric model of the ISAC-enabled UAV HO process.

RSRP-based criterion, the proposed joint HO criterion reduces the HO region length by 49.97% and improves the HO activation probability by 76.31% when signal-to-noise ratio (SNR) is greater than 0 dB and the sensing pilot ratio is 20%. Furthermore, it maintains performance improvements under low SNR and low sensing pilot ratio conditions.

The remainder of this paper is organized as follows: Section II establishes the ISAC signal model and derives the CRLB for distance sensing. Section III proposes the HO criterion. Section IV provides performance simulations. Section V concludes the paper.

II. SYSTEM MODEL

In this section, we establish the ground-to-air (G2A) geometric model, the ISAC signal model, and derive the CRLB for distance estimation.

A. G2A Geometric Model

In LAWNs, the HO process of a UAV from the serving BS to the target BS is shown in Fig. 1. Without loss of generality, we establish a three-dimensional (3D) Cartesian coordinate system with the midpoint between the serving BS and the target BS as the origin, and the positive x -axis pointing toward the target BS. The antenna coordinates of the two BSs are $(-x_{BS}, 0, h_{BS})$ and $(x_{BS}, 0, h_{BS})$, respectively, while the UAV is located at (x, y, h_{AV}) ¹. Let d_S and d_T denote the Euclidean distances from the UAV to the serving BS and the target BS, respectively, then $d_S = \sqrt{(x + x_{BS})^2 + y^2 + (h_{AV} - h_{BS})^2}$ and $d_T = \sqrt{(x - x_{BS})^2 + y^2 + (h_{AV} - h_{BS})^2}$.

B. ISAC Signal Model

Assume that each BS is equipped with a uniform planar array (UPA) with $N_t = N_x N_y$ antenna elements, while the UAV employs a single omnidirectional antenna. The BS transmits an orthogonal frequency-division multiplexing (OFDM) waveform that simultaneously enables communication and sensing, expressed as [8]

$$s(t) = \sum_{m=0}^{M-1} \sum_{n=0}^{N-1} \sqrt{P_{\text{sub}}} d_{m,n} e^{j2\pi(f_c + n\Delta f)t} \text{rect}\left(\frac{t - mT}{T}\right), \quad (1)$$

¹Given the short duration of the HO process, the impact of UAV velocity on HO decisions is negligible compared to that of distance. Therefore, as a preliminary study, this paper does not consider UAV mobility during the HO decision-making procedure, which will be explored in future work.

where M and N denote the number of OFDM symbols and subcarriers, respectively. The power allocated to the n -th subcarrier is P_{sub} , with uniform power allocation assumed [9], i.e., $P_{\text{sub}} = \frac{P_{\text{sum}}}{N}$, where P_{sum} represents the total transmit power. The modulation symbols $d_{m,n}$ satisfy the normalization condition $\mathbb{E}[|d_{m,n}|^2] = 1$. We define the sensing subcarrier ratio $\rho \in (0, 1]$ to represent the proportion of subcarriers used for sensing. Thus, given a total system bandwidth B , the sensing bandwidth is $B_S = \rho B$, and the communication bandwidth is $B_C = (1 - \rho)B$. The carrier frequency is f_c , and the subcarrier spacing is $\Delta f = \frac{B}{N}$. The duration of each OFDM symbol is $T = T_u + T_{\text{CP}}$, where $T_u = \frac{1}{\Delta f}$ is the useful symbol duration and T_{CP} is the cyclic prefix duration. The function $\text{rect}(\cdot)$ represents a rectangular window used to limit the symbol duration.

For BS in full-duplex or time domain half-duplex mode, the signal transmitted by the BS is reflected by the target UAV and received by the same BS for parameter estimation, and its time-domain expression is given by

$$r(t) = \sum_{m=0}^{M-1} \sum_{n=0}^{N-1} \sqrt{P_{\text{sub}}} \mathbf{h}_{m,n}^H \mathbf{w} d_{m,n} e^{j2\pi(f_c + n\Delta f)t} \times \text{rect}\left(\frac{t - \tau_S - mT}{T}\right) + n(t), \quad (2)$$

where $\tau_S = \frac{2d}{c}$ is the round-trip delay, c is the speed of light, and $n(t) \sim \mathcal{CN}(0, \sigma^2)$ is the channel noise. $\mathbf{h}_{m,n}^H$ is the frequency-domain response of the sensing link at the n -th subcarrier and the m -th OFDM symbol, given by $\mathbf{h}_{m,n}^H = \sqrt{\beta_S} e^{-j2\pi n \Delta f \tau_S} \mathbf{v}^H$, where $\sqrt{\beta_S} = 10^{-\frac{2\mathcal{L} + \varepsilon}{20}}$ is the sensing path gain, which accounts for the two-way path loss $2\mathcal{L}$ and the shadow fading term $\varepsilon \sim \mathcal{N}(0, \sigma_{\text{SF}}^2)$. At typical UAV flight altitudes of 100 to 300 m, the LoS probability approaches 100% [10]. Consequently, only the LoS path between the BS and UAV is considered, with path loss is modeled using the 3GPP UMa-AV LoS model [10] as $\mathcal{L} = 28.0 + 22\log_{10}(d) + 20\log_{10}(f_c)$, where d is in meters and f_c is in GHz². Additionally, as a preliminary study, we assume beam alignment for ISAC signal transmission, where the transmit beam direction $\mathbf{w} \in \mathbb{C}^{N_x N_y \times 1}$ is aligned with the UAV's array response vector $\mathbf{v}^H \in \mathbb{C}^{1 \times N_x N_y}$, i.e., $\mathbf{w} = \mathbf{v}$. In this case, the beamforming gain is $G = |\mathbf{v}^H \mathbf{w}|^2 = N_t^2$.

By sampling the echo signal $r(t)$, removing the cyclic prefix, and performing an N -point fast Fourier transform, the resulting frequency-domain samples are given by

$$r_{m,n} = \sqrt{P_{\text{sub}} \beta_S} N_t d_{m,n} e^{-j2\pi n \Delta f \tau_S} + n_{m,n}. \quad (3)$$

For the communication link, its frequency-domain channel model can be expressed as $\tilde{\mathbf{h}}_{m,n}^H = \sqrt{\beta_C} e^{-j2\pi n \Delta f \tau_C} \mathbf{v}^H$, where $\tau_C = \frac{d}{c}$ is the one-way propagation delay, and $\sqrt{\beta_C} = 10^{-\frac{\mathcal{L} + \varepsilon}{20}}$ is the large-scale gain. The received power at the UAV is $P = \beta_C N_t^2 P_{\text{sum}}$, with its logarithmic form (dBm) as $P = P_{\text{sum}} + 20\log_{10} N_t - \mathcal{L} - \varepsilon$. Additionally, the corresponding data rate R is given by [11]

$$R = (1 - \rho) B \log_2 \left(1 + \frac{\beta_C N_t^2 P_{\text{sum}}}{N \sigma^2} \right). \quad (4)$$

²For distances below 100 m, the probability of non-line-of-sight (NLoS) conditions increases, for which the UMa-AV NLoS model is adopted.

C. CRLB Derivation

Define the equivalent channel gain as $\alpha \triangleq \sqrt{P_{\text{sub}}\beta_S N_t}$, and the phase factor as $A_n \triangleq 2\pi n\Delta f$. Assuming that the noise $n_{m,n}$ is i.i.d. circularly symmetric complex Gaussian, the likelihood function of the observation vector \mathbf{r} parameterized by the time delay τ_S is given by

$$L(\mathbf{r}|\tau_S) = \prod_{m=0}^{M-1} \prod_{n \in \mathcal{S}_m} \left[\frac{1}{\sqrt{2\pi\sigma^2}} e^{-\frac{1}{2\sigma^2} (r_{m,n} - \alpha d_{m,n} e^{-jA_n \tau_S})^2} \right], \quad (5)$$

where \mathcal{S}_m denotes the set of subcarrier indices allocated for sensing in the m -th OFDM symbol, with $|\mathcal{S}_m| = \rho N$.

Taking the logarithm of (5) and computing its second-order derivative with respect to τ_S , the Fisher information $\mathbf{J}(\tau_S)$ is obtained as [12]

$$\begin{aligned} \mathbf{J}(\tau_S) &= -\mathbb{E} \left[\frac{\partial^2 \ln(L(\mathbf{r}|\tau_S))}{\partial \tau_S^2} \right] \\ &= \frac{\alpha}{\sigma^2} \sum_{m=0}^{M-1} \sum_{n \in \mathcal{S}_m} A_n^2 E \left[\text{Re} \{ d_{m,n} r_{m,n}^* e^{-jA_n \tau_S} \} \right]. \end{aligned} \quad (6)$$

According to $\mathbf{J}(\tau_S)$, the mean squared error of the time delay estimation satisfies $\text{Var}(\hat{\tau}_S) \geq \frac{1}{\mathbf{J}(\tau_S)}$. Given the propagation model, the distance estimation is $\hat{d} = \frac{c\hat{\tau}_S}{2}$, and its CRLB is $\text{CRLB}(d) = \frac{c^2}{4\mathbf{J}(\tau_S)}$. To relate estimation accuracy to the SNR, the average per-subcarrier SNR is defined as $\gamma = \frac{\beta_S N_t^2 P_{\text{sum}}}{N\sigma^2}$. Thus, $\text{CRLB}(d)$ can be rewritten as

$$\text{CRLB}(d) = \frac{3c^2}{8\pi^2 \gamma \Delta f^2 M \rho N (\rho N - 1) (2\rho N - 1)}. \quad (7)$$

Remark 1. *The theoretical lower bound $\text{CRLB}(d)$ of distance estimation in (7) provides a theoretical foundation for the subsequent performance analysis of HO criteria. When $\rho N \geq 1$, considering $\Delta f = \frac{B}{N}$ and $B_S = \rho B$, the lower bound can be approximated as $\text{CRLB}(d) \approx \frac{3c^2}{16\pi^2 \gamma \rho M N B_S^2}$, indicating that sensing accuracy is inversely proportional to γ , ρ , M , N , and B_S^2 , with particularly strong sensitivity to the sensing bandwidth B_S .*

Assuming that the BS's distance estimation could achieve the CRLB and the estimation error follows a Gaussian distribution, i.e., $\epsilon \sim \mathcal{N}(0, \text{CRLB}(d))$, the estimated distance is modeled as $\hat{d} \sim \mathcal{N}(d, \text{CRLB}(d))$.

III. HO CRITERION AND PERFORMANCE METRICS

To enhance HO reliability, we propose a joint HO criterion that integrates the ISAC-based sensing information with the traditional RSRP-based mechanism. In the conventional RSRP-based HO criterion, the A3 event was adopted as the activation condition [4], where an HO is triggered when the received power P_T from the target BS exceeds that from the serving BS P_S by a hysteresis threshold Γ , with the HO activation probability $\mathbb{P}_{\text{HO}}^{\text{RSRP}}$ given by [6]

$$\mathbb{P}_{\text{HO}}^{\text{RSRP}} = \mathbb{P}[P_T - P_S > \Gamma] = Q\left(\frac{\Gamma + \mathcal{L}(d_T) - \mathcal{L}(d_S)}{\sqrt{2}\sigma_{SF}}\right). \quad (8)$$

In cellular networks, multipath fading and blockage hinder accurate user localization, prompting HO decisions to rely primarily on instantaneous communication measurements. In UAV scenarios, however, the dominance of LoS links yields a more stable and observable spatial relationship between the UAV and BSs, rendering distance a reliable basis for HO decisions. Based on this insight, we propose that HO can be triggered when the estimated distance \hat{d}_S to the serving BS exceeds that to the target BS \hat{d}_T by more than a threshold d_{th} , with the HO activation probability $\mathbb{P}_{\text{HO}}^{\text{dist}}$ given by

$$\begin{aligned} \mathbb{P}_{\text{HO}}^{\text{dist}} &= \mathbb{P}[\hat{d}_S - \hat{d}_T > d_{\text{th}}] \\ &= Q\left(\frac{d_{\text{th}} + d_T - d_S}{\sqrt{\text{CRLB}(d_T) + \text{CRLB}(d_S)}}\right). \end{aligned} \quad (9)$$

To improve the robustness of HO decisions, we combine the sensing-based and RSRP-based criteria to form a joint HO mechanism, which triggers an HO when either condition is met, and the activation probability $\mathbb{P}_{\text{HO}}^{\text{joint}}$ is given by

$$\begin{aligned} \mathbb{P}_{\text{HO}}^{\text{joint}} &= \mathbb{P}[(P_T - P_S > \Gamma) \cup (\hat{d}_S - \hat{d}_T > d_{\text{th}})] \\ &= \mathbb{P}_{\text{HO}}^{\text{RSRP}} + \mathbb{P}_{\text{HO}}^{\text{dist}} - \mathbb{P}_{\text{HO}}^{\text{RSRP}} \cdot \mathbb{P}_{\text{HO}}^{\text{dist}}. \end{aligned} \quad (10)$$

To evaluate HO performance comprehensively, we introduce the effective data rate R_{eff} , which captures both activation probability and data rate, defined as

$$R_{\text{eff}} = (1 - \mathbb{P}_{\text{HO}})R_S + \mathbb{P}_{\text{HO}}R_T, \quad (11)$$

where R_S and R_T denote the data rates when connected to the serving and target BSs, respectively. $(1 - \mathbb{P}_{\text{HO}})R_S$ and $\mathbb{P}_{\text{HO}}R_T$ are the data rates before and after HO, respectively.

IV. PERFORMANCE EVALUATION

A. Simulation Parameter Settings

To evaluate the performance of different HO criteria, we simulate the UAV flying along the x -axis from the serving BS to the target BS at different altitudes as shown in Fig. 1, with the simulation parameters listed in Table I³. According to (8)–(10), the HO activation probability is shown to be a function of position, denoted as $\mathbb{P}_{\text{HO}} = f(x)$. We define the x -axis range corresponding to $P_{\text{HO}} \in [0.1, 0.9]$ as the HO region $D_{\text{HO}} = [f^{-1}(0.1), f^{-1}(0.9)]$, and its length is defined as the HO region length, given by $L_{\text{HO}} = |f^{-1}(0.9) - f^{-1}(0.1)|$.

B. Simulation Analysis

1) *Comparison of HO Activation Probability Distributions under Different HO Criteria:* Fig. 2 shows the distribution of HO activation probabilities for RSRP-based, sensing-based, and joint HO criteria at $h_{\text{AV}} = 200$ m. First, under the RSRP-based HO criterion, the HO region exhibits the widest spatial distribution, with a statistical range of $D_{\text{HO}} = [-26, 469]$ m, corresponding to a length of 495 m. Moreover, L_{HO} increases from 238 m to 495 m as $|y|$ increases. In contrast, the HO

³To preliminarily evaluate the proposed HO scheme, a simplified UAV trajectory is considered. More complex UAV mobility patterns, such as 3D maneuvers and agile directional changes, will be explored in future work.

TABLE I
THE MAIN SIMULATION PARAMETERS

Parameters	Value
Carrier frequency f_c	2 GHz [4]
System bandwidth B	10 MHz [4]
Transmission power of BS	46 dBm [4]
BS antenna configuration $N_x \times N_y$	8×4 [4]
Coordinates of the serving BS antenna	(-1000, 0, 25) m
Coordinates of the target BS antenna	(1000, 0, 25) m
UAV altitude range	(100, 300) m [4]
UAV antenna configuration	Omni-directional
Number of OFDM symbols M	64 [13]
Number of subcarriers N	50 [13]
Sensing pilot ratio ρ	20%
Subcarrier spacing Δf	200 kHz
Duration of the effective symbol T_u	$5 \mu\text{s}$
Duration of the cyclic prefix T_{CP}	$1.25 \mu\text{s}$
Duration of the OFDM symbol T	$6.25 \mu\text{s}$
Speed of light c	3×10^8 m/s
Shadow fading σ_{SF}	$4.64 \exp(-0.0066 h_{AV})$ dB [4]
RSRP hysteresis Γ	2 dB [4]
Distance threshold d_{th}	50 m
Noise power σ^2	-100 dB

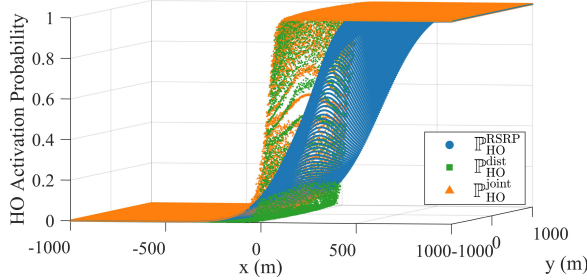


Fig. 2. Distributions of HO activation probability under different HO criteria.

region under the sensing-based criterion is more concentrated, with a range of $D_{HO} = [3, 67]$ m, corresponding to a length of 64 m. Finally, the joint HO criterion strikes a balance between the two, with a HO range of $D_{HO} = [-31, 67]$ m, corresponding to a length of 98 m. Additionally, L_{HO} increases from 43 m to 92 m as $|y|$ increases. Overall, the joint HO criterion retains the early activation of the RSRP-based HO criterion while leveraging the spatial consistency and sensitivity of the sensing-based HO criterion, achieving a balanced trade-off between HO responsiveness and stability.

2) *Comparison of HO Activation Behavior under Different Thresholds:* Fig. 3 shows the HO activation probability of the RSRP-based and the joint HO criteria under different HO triggering thresholds along the x -axis ($y = 0, h_{AV} = 200$ m). First, under the RSRP-based HO criterion, as Γ increases from 0 to 2 dB, the lower boundary of the HO region D_{HO} shifts from $x = -120$ m to $x = -13$ m, with a displacement of 107 m. The corresponding L_{HO} remains relatively large in all configurations. Second, under the joint HO criterion, despite d_{th} spanning a wide range of 0–100 m, the lower boundary of the D_{HO} remains consistently around $x = -13$ m, and L_{HO} stays within a consistently small range across all configurations. We note that the joint HO criterion maintains a stable lower boundary and shorter HO region length under varying thresholds, demonstrating stronger robustness than the RSRP-based criterion.

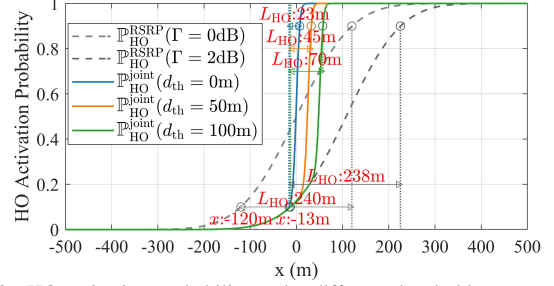


Fig. 3. HO activation probability under different thresholds.

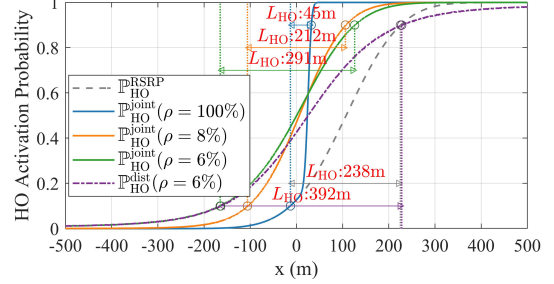


Fig. 4. HO activation probability under different sensing pilot ratios.

3) *Comparison of HO Activation Behavior under Different Sensing Pilot Ratios:* Fig. 4 shows the HO activation probability of the joint HO criterion along the x -axis ($y = 0, h_{AV} = 200$ m) under different sensing pilot ratios ρ . First, As ρ increases, the L_{HO} of the joint HO criterion exhibits a decreasing trend, indicating that the sensing distance parameter contributes to the improvement of HO performance. Second, when $\rho \geq 8\%$, the L_{HO} of joint HO criterion consistently remains lower than that of the traditional RSRP-based criterion, demonstrating superior performance in HO distance control. Finally, when ρ decreases to 6%, the L_{HO} of the sensing-based HO criterion reaches 393 m, while that of the joint HO criterion increases to 290 m, which is slightly higher than the RSRP-based criterion (238 m) but remains at a comparable level. It is observed that under low sensing pilot ratio conditions, the joint HO criterion mitigates the expansion of the HO region by incorporating RSRP, compensating for degraded distance estimation accuracy.

4) *Comparison of Average HO Region Lengths under Different Altitudes:* Fig. 5 shows the average HO region length L_{HO} on the x - y plane under different altitudes h_{AV} , for both RSRP-based and joint HO criteria. As altitude increases, L_{HO} of both HO criteria decreases: L_{HO} of the RSRP-based HO criterion drops from 614 m to 167 m, while L_{HO} of the joint HO criterion decreases from 270 m to 139 m. We note that the joint HO criterion consistently yields a smaller HO region length, with a 49.97% average reduction in 3D space compared to the RSRP-based HO criterion.

5) *Comparison of Average HO Activation Probability Improvement under Different SNR conditions:* Fig. 6 shows the average improvement in HO activation probability of the sensing-based and joint HO criteria over the RSRP-based criterion under various SNRs within the 3D HO region. In the high SNR region ($\text{SNR} \geq 0$ dB), the activation probability improvements of both HO criteria tend to stabilize, with the joint HO and sensing-based HO criteria reaching 76.31% and

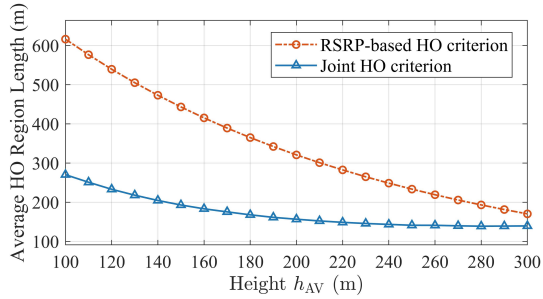


Fig. 5. Average HO region length L_{HO} under different altitudes.

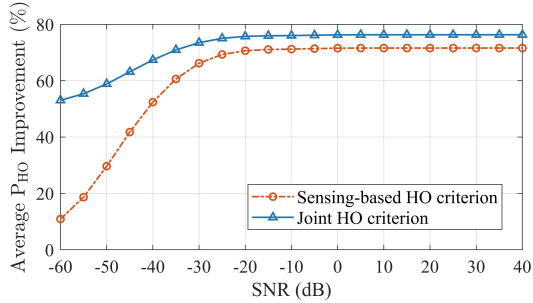


Fig. 6. Average HO activation probability improvement under different SNR conditions.

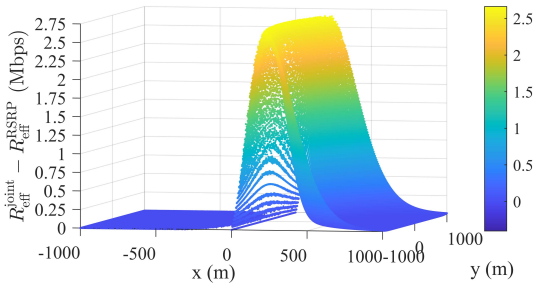


Fig. 7. Distribution of the effective data rate difference between the joint HO criterion and the RSRP-based HO criterion.

71.60%, respectively. As the SNR decreases, the improvements of both criteria decline, and the performance gap gradually widens, while the joint HO criterion exhibits a smaller rate of decline. This can be explained by the theoretical lower bound: according to (7), when $SNR \leq -40$ dB, the CRLB rises to 10^2 , making limited sensing accuracy a major constraint on the performance of the sensing-based HO criterion. In comparison, the joint HO criterion improves the HO activation probability by leveraging the sensing distance parameter, while the inclusion of the SNR-insensitive RSRP enables it to maintain a high activation probability even under degraded observation accuracy and exhibiting stronger noise robustness.

6) *Analysis of Data Rate Improvement:* Beyond HO performance, the joint HO criterion also offers advantages in key service metrics, such as data rate. Fig. 7 shows the spatial distribution of the effective data rate difference $R_{eff}^{joint} - R_{eff}^{RSRP}$ between the joint HO criterion and the RSRP-based HO criterion at $h_{AV} = 200$ m. The advantage of the joint HO criterion is primarily concentrated within the HO region, where the maximum data rate difference reaches 2.67 Mbps; outside the HO region, the data rate of both criteria is nearly identical. This indicates that the joint HO criterion enhances transmission performance within the HO region.

V. CONCLUSION

To address the issue of redundant HOs or HO failures caused by the RSRP-based HO criterion in cellular-connected UAV scenarios, we propose an HO criterion that integrates ISAC sensing information with RSRP to enhance HO performance. First, a low-altitude ISAC signal model is established, and the CRLB for distance estimation is derived. Based on this, we design a sensing-based HO criterion and integrate it with the RSRP-based HO criterion to form a joint HO criterion. Simulation results show that under conditions of $SNR \geq 0$ dB and a sensing pilot ratio of 20%, the proposed joint HO criterion improves the handover activation probability by 76.31% and reduces the HO region length by 49.97%, significantly outperforming the baseline RSRP-based criterion. Moreover, even under challenging scenarios such as low SNR and reduced sensing pilot ratios, the proposed method maintains stable HO performance, demonstrating strong robustness.

This paper initially demonstrates the feasibility of sensing-assisted HO in cellular-connected LAWNs, and future work will further consider UAV mobility, flight trajectories, and ping-pong HOs to design and improve HO schemes.

REFERENCES

- [1] F. Liu, Y. Cui, C. Masouros, J. Xu, T. X. Han, Y. C. Eldar, and S. Buzzi, "Integrated Sensing and Communications: Toward Dual-Functional Wireless Networks for 6G and Beyond," *IEEE Journal on Selected Areas in Communications*, vol. 40, no. 6, pp. 1728–1767, 2022.
- [2] K. Meng, C. Masouros, A. P. Petropulu, and L. Hanzo, "Cooperative ISAC Networks: Opportunities and Challenges," *IEEE Wireless Communications*, 2024.
- [3] Y. Ma, A. Shafie, J. Yuan, G. Ma, Z. Zhong, and B. Ai, "Orthogonal Delay-Doppler Division Multiplexing Modulation with Tomlinson-Harashima Precoding," *IEEE Transactions on Communications*, 2024.
- [4] 3rd Generation Partnership Project (3GPP), "NR; Radio Resource Control (RRC); Protocol specification (Release 16)," Tech. Rep. TS 38.331, 3GPP, 2020.
- [5] Y. Jang, S. M. Raza, H. Choo, and M. Kim, "UAVs Handover Decision using Deep Reinforcement Learning," in *2022 16th International Conference on Ubiquitous Information Management and Communication (IMCOM)*, pp. 1–4, IEEE, 2022.
- [6] B. Hu, H. Yang, L. Wang, and S. Chen, "A Trajectory Prediction based Intelligent Handover Control Method in UAV Cellular Networks," *China Communications*, vol. 16, no. 1, pp. 1–14, 2019.
- [7] Y. Ge, O. Kallio, H. Chen, J. Talvitie, Y. Xia, G. Madhusudan, G. Larue, L. Svensson, M. Valkama, and H. Wymeersch, "Target Handover in Distributed Integrated Sensing and Communication," *arXiv preprint arXiv:2411.01871*, 2024.
- [8] Y. Ma, B. Ai, G. Ma, A. Shafie, Q. Cheng, M. Yang, J. Li, X. Pang, J. Yuan, and Z. Zhong, "Channel Spreading Function-Inspired Channel Transfer Function Estimation for OFDM Systems with High-Mobility," *IEEE Wireless Communications Letters*, 2025.
- [9] G. Bansal, M. J. Hossain, and V. K. Bhargava, "Optimal and Suboptimal Power Allocation Schemes for OFDM-based Cognitive Radio Systems," *IEEE Transactions on Wireless Communications*, vol. 7, no. 11, pp. 4710–4718, 2008.
- [10] 3rd Generation Partnership Project (3GPP), "Technical Report TR 36.777: Enhanced LTE Support for Aerial Vehicles," Tech. Rep. TR 36.777, 3GPP, Dec 2018. Release 15.
- [11] C. E. Shannon, "A Mathematical Theory of Communication," *The Bell System Technical Journal*, vol. 27, no. 3, pp. 379–423, 1948.
- [12] C. Mensing, *Location Determination in OFDM based Mobile Radio Systems*. PhD thesis, Technische Universität München, 2013.
- [13] L. Gaudio, M. Kobayashi, B. Bissinger, and G. Caire, "Performance Analysis of Joint Radar and Communication using OFDM and OTFS," in *2019 IEEE International Conference on Communications Workshops (ICC Workshops)*, pp. 1–6, IEEE, 2019.